Theor Chem Acc (2007) 117:603–619
DOI 10.1007/s00214-006-0196-z

REGULAR ARTICLE

Computational NMR spectroscopy: reversing the information flow

Alessandro Bagno · Giacomo Saielli

Received: 4 September 2006 / Accepted: 13 October 2006 / Published online: 19 December 2006

Abstract Work on computational NMR recently carried out at our Laboratory in Padova is reviewed. We summarize our results concerning the calculation of NMR properties (chemical shifts and spin–spin coupling constants) in a variety of contexts, from the structure elucidation of complex organic molecules or molecules containing heavy atoms to weakly interacting species, such as those involved in hydrogen bonding or van der Waals CH-π interactions. We also present some original results, viz. the calculated ^{1}H and ^{13}C spectra of the putative natural substance nimbosodione, the first examples of calculated ^{181}Ta chemical shifts, spin–spin couplings in Hg_4^{2+} and through-space coupling constants involving ^{205}Tl.

Keywords Density functional theory · Relativistic calculations · NMR spectroscopy · Chemical shift · Spin–spin coupling

1 Introduction

Nuclear magnetic resonance spectroscopy has rightly acquired the status of an indispensable tool in all areas of chemistry, and has become a discipline in its own right. The prominent role of this technique stems from the wealth of information that can be gleaned, which spans both structure and dynamics; indeed, NMR has become a staple methodology for the determination of the structure of organic and inorganic species. Moreover, its sensitivity to long-range environmental effects, such as solvation and weak interactions at large, further widens its scope of applicability (or, depending on the viewpoint, complicates the interpretation of the data) [1].

The basic pieces of information that one can get from NMR spectroscopy are chemical shifts, coupling constants and relaxation rates. Each quantity probes into different physico-chemical phenomena (although the boundaries are obviously blurred).

Thus, chemical shifts yield information on the chemical environment of a given nucleus; as such, this is the fundamental building block of any NMR investigation. Spin–spin coupling, thanks to its well-known property of rapidly vanishing with increasing number of covalent bonds, provides through-bond connectivities and hence the backbone of molecular structures. Traditionally a staple technique of conformational analysis, the scope of spin–spin coupling has been further enhanced by the recognition that weak couplings can exist even in the absence of "real" chemical bonding [1].

Relaxation rates simultaneously depend on (and probe into) both structural and dynamical features. On one hand, this constitutes a natural avenue for investigating molecular dynamics; on the other hand it enforces certain limitations on the extent of structural information that can be obtained, for example in the case of relaxation of quadrupolar nuclei. This is because solution dynamics depend to a large extent on collective rather than molecular properties; thus, the relaxation rate of quadrupolar nuclei depends on the combined influence of the electric field gradient (a molecular

A. Bagno (✉)
Dipartimento di Scienze Chimiche,
Universitá di Padova, via Marzolo 1, 35131 Padova, Italy
e-mail: alessandro.bagno@unipd.it

G. Saielli
Istituto CNR per la Tecnologia delle Membrane,
Sezione di Padova, Padova, Italy

property) and the correlation time of its fluctuations (an essentially bulk property). The problems inherent to this approach are reviewed in [2].

Since we are interested in the computational modeling of NMR properties of molecules, in this article we will not discuss relaxation rates despite the utmost importance of associated effects like the NOE. As we will shortly see, however, restricting the scope to "just" chemical shifts and couplings brings in an incredible quantity of information (and problems).

Even though we are still witnessing a steady advancement in NMR techniques, the rich information provided may not lead to an unambiguous solution of structural problems. This holds both for organic (owing to their extraordinary complexity) and inorganic molecules (owing to the presence of little-studied nuclei). There is indeed a large number of challenging problems where, despite a "brute-force" approach, a structural elucidation has proved difficult—viz. for example the recent review by Nicolaou and Snyder on "Molecules That Never Were" [3].

In the course of the last decade we have been deeply involved in approaching the problem from the other end—trying to predict NMR properties a priori rather than striving to extract information from spectra. It is the purpose of this article to show the degree of accuracy and understanding that can be achieved in a wide array of chemical problems. Before going into the matter, we will briefly recapitulate some fundamentals of the physical quantities that ultimately dictate the appearance of an NMR spectrum.

The chemical shift (δ) of a given nucleus in a molecule is expressed by $\delta = \sigma_{\mathrm{ref}} - \sigma$, where σ is the isotropic part of the shielding tensor σ of the molecule of interest and of one conventionally taken as reference (e.g. TMS). In turn, the shielding constant is the sum of at least two contributions called the diamagnetic (σ_{d}) and paramagnetic (σ_{p}) shieldings, so that $\sigma = \sigma_{\mathrm{d}} + \sigma_{\mathrm{p}}$. Although these two terms are sufficient for describing the shielding in molecules where only light nuclei are present, heavy atoms are substantially influenced by relativistic effects and may even induce additional effects in light nuclei bonded to them; whereby a third term, called spin–orbit shielding, has to be added ($\sigma = \sigma_{\mathrm{d}} + \sigma_{\mathrm{p}} + \sigma_{\mathrm{so}}$).

J-coupling is indirectly transmitted by bonding electrons through a variety of interactions: Fermi Contact (FC), often the largest contribution, diamagnetic spin–orbit (DSO), paramagnetic spin–orbit (PSO) and spin-dipole (SD), so that in general $J = J^{\mathrm{FC}} + J^{\mathrm{DSO}} + J^{\mathrm{PSO}} + J^{\mathrm{SD}}$.

Modern quantum chemistry methods, and especially density-functional theory, have enabled the computation of the relevant quantities with considerable accuracy [4,5]. Indeed, the last decade has seen the progress in the calculation of NMR properties from a very specialized technique into something close to just another computational tool for structure elucidation. Thus, in parallel with its remarkable success, the relevant routines have been incorporated into most popular quantum-chemistry packages and made available to the wide community of chemists and NMR spectroscopists.

Our own interest in these methodologies arose from our long-standing involvement in the NMR of heteronuclei. A major difficulty inherent to this area of NMR stems from the fact that for nuclei other than ^{1}H, ^{13}C and few others the knowledge base is very limited. Furthermore, chemical shifts of many heteronuclei span thousands of parts per million and respond to structural changes in an unpredictable or counterintuitive manner, as we have shown for the changes induced by proton transfer in amide compounds [2]. The invaluable help we received from the computational approach led us to believe that the scope could be made substantially broader.

In this connection, a thought arises naturally: is it possible to completely predict an NMR spectrum in the same way that, for example, a structure is predicted for an elusive molecular species? Little reflection is needed to appreciate that, in order to do this, one should "just" be able to calculate the shieldings and couplings for all nuclei of interest—which of course raises the further question, whether current theoretical methods are up to the expectations. If we imagine that this is the case we could work backwards, from molecular structure to NMR spectrum rather than vice versa as is normally done. In other words, one could start from one or few molecular structures viable for the problem at hand, compute NMR spectra for each and compare the calculated spectra with the experimental one, as sketched in Scheme 1. This amounts to effectively reverse the information flow of NMR.

With this aim in mind, since the very beginning we strived to approach the problem in a comprehensive way, i.e. simultaneously calculating both chemical shifts *and* coupling constants. (While this idea seems straightforward now, it must be remarked that the calculation of coupling constants has always been comparatively less advanced, so at that time only chemical shift calculations were in fairly common use.)

This paper will then present various areas of application where we have found the calculation of NMR properties as useful and stimulating methodology. As we will see, the scope embraces straightforward applications, such as structure elucidation and conformational analysis, as well as less obvious ones like the study of weak interactions.

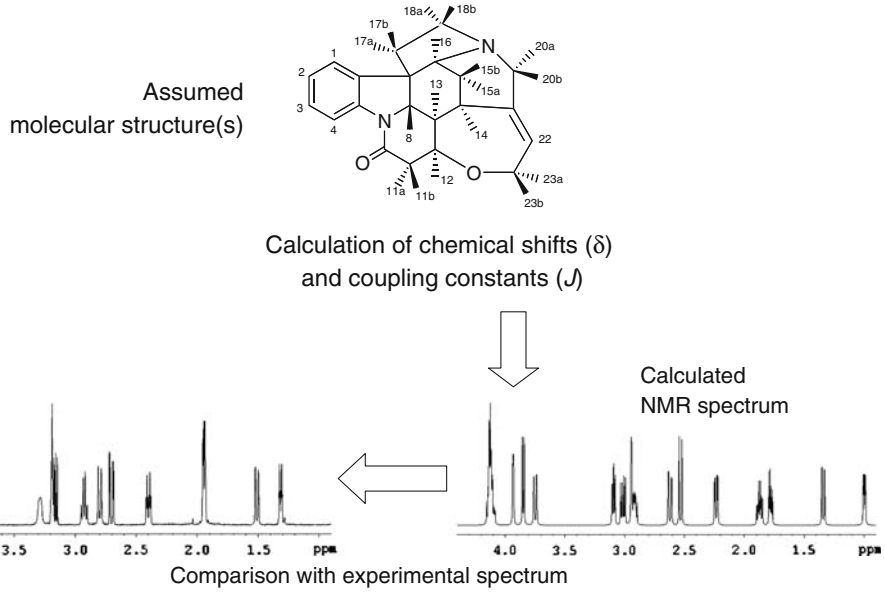

Scheme 1 A thought experiment in computational NMR

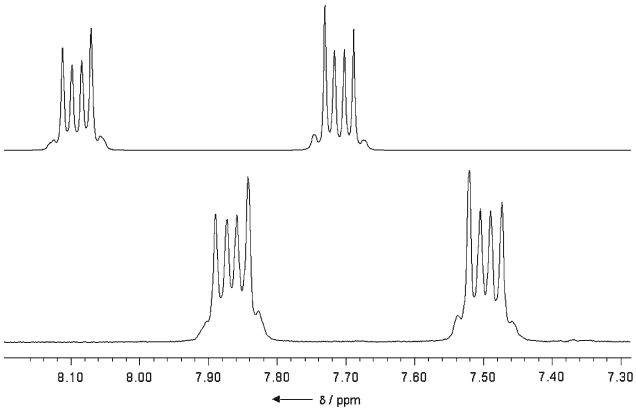

Fig. 1 Experimental (*bottom*) and calculated (*top*) (B3LYP/cc-pVTZ//6-31G(d,p)) ^{1}H spectrum of naphthalene. Reproduced with permission from Ref. [6]. © 2001 Wiley-VCH

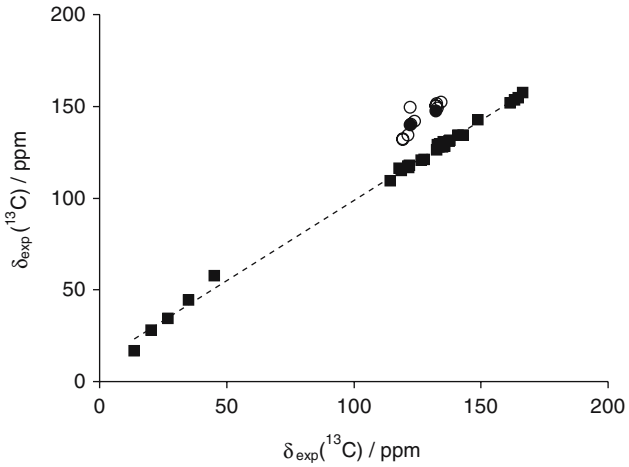

Fig. 2 Experimental and calculated ^{13}C chemical shifts. Circles denote data points for halogen-bound carbons. Fit parameters of $\delta_{\mathrm{calc}} = a\delta_{\mathrm{exp}} + b$ (excluding the outliers): $a = 0.874, b = 11.2$ ppm, $r^2 = 0.997$. Data from Ref. [7]

2 Predicting the NMR spectra of organic molecules

The first implementation concerned the ^{1}H NMR spectra of simple organic molecules [6]. After extensive testing, we proposed the use of the popular B3LYP functional for geometry optimization (with the 6-31G(d,p) basis) and for NMR calculations (with the cc-pVTZ basis), although other functionals performed similarly. In these early stages, the study was restricted to conformationally rigid, non-polar molecules to avoid further complications.

By examining a fairly wide sample of organic functionalities, the following major points emerged. (a) DFT calculations can predict most features of typical 1D NMR spectra with outstanding accuracy. (b) The calculation of proton couplings is simplified because the DSO and PSO terms, although they are comparable in magnitude to FC, cancel out and therefore $J \approx J^{\mathrm{FC}}$ (the SD term is negligible anyway).

The definitive answer to the question whether or not such an accuracy is at all useful in common NMR practice is provided by a straightforward visual comparison

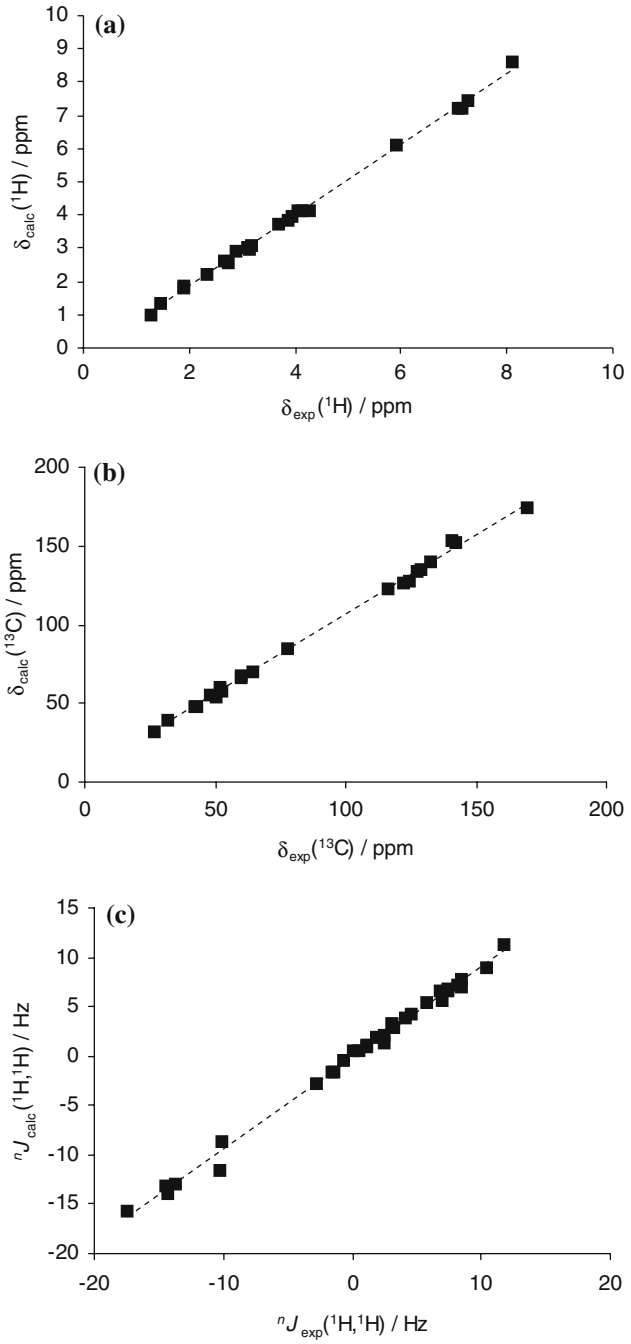

Fig. 3 Experimental and calculated (B3LYP/cc-pVTZ//6-31G(d,p)) NMR properties of strychnine. **a** ^{1}H chemical shifts; fit parameters of $\delta_{\mathrm{calc}} = a\delta_{\mathrm{exp}} + b : a = 1.07, b = -0.27\,\mathrm{ppm}, r^2 = 0.998$. **b** ^{13}C chemical shifts; fit parameters of $\delta_{\mathrm{calc}} = a\delta_{\mathrm{exp}} + b : a = 1.01, b = 5\,\mathrm{ppm}, r^2 = 0.998$. **c** J(H,H) coupling constants; fit parameters of $J_{\mathrm{calc}} = aJ_{\mathrm{exp}} + b : a = 0.93, b = 0.17\,\mathrm{Hz}, r^2 = 0.994$. Data from Ref. [15]

of the experimental spectrum with one simulated from calculated shifts and couplings, as is done in Fig. 1 for naphthalene. The calculation reproduces the appearance of the complex multiplets arising from its very complicated spin system ($\mathrm{AA'A''A'''BB'B''B'''}$).

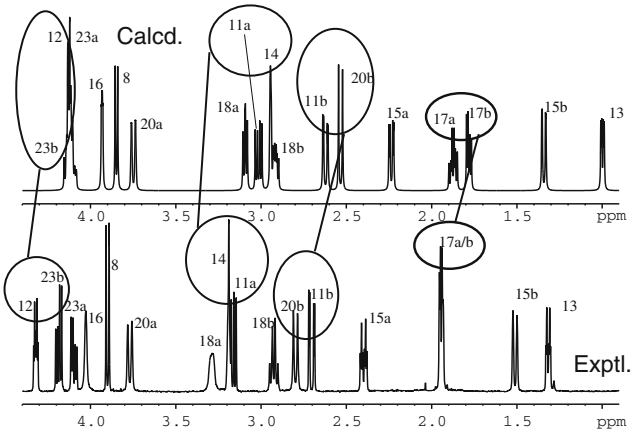

Fig. 4 Calculated (B3LYP/cc-pVTZ//6-31G(d,p)) and experimental ^{1}H spectrum of strychnine (aliphatic region). Inversions between calculated and experimental resonances are highlighted. Reproduced with permission from Ref. [15]. © 2006 Wiley-VCH

^{13}C is the next step of any structural work on organic species; the wide array of experimental techniques available provides (in principle) the entire carbon framework and connectivity pattern with directly bonded and long-range protons. The computational study of ^{13}C chemical shifts and ^{n}J(C,H) couplings logically follows [7]. In Fig. 2 we show the correlation plot between calculated and experimental ^{13}C chemical shifts.

Although the general accuracy of these results is quite similar to that found for ^{1}H, one cannot fail to notice a group of data points systematically lying above the correlation line of Fig. 2. These points pertain to carbon atoms directly bonded to halogen atoms (Cl, Br), and considerable (but rewarding) effort was put into understanding the origin of this discrepancy. An outstanding deviation is displayed by *ortho*-bromochlorobenzene (OBCB), whose six carbons resonate in a narrow 12-ppm range, in the order C6 ≈ C2 > C3 > C4 > C5 > C1 (C1 and C2 being, respectively, bonded to Br and Cl). The large shielding of C1 is not expected on the basis of simple electronic effects, but is rather reminiscent of analogous stronger effects known to occur when carbon is bonded to several heavy halogen atoms. The best-known such example is perhaps that of CI_4, where ^{13}C resonates at $\delta = -290$ ppm, i.e. far outside its typical range. This effect is now known to arise from relativistic spin–orbit effects due to the heavy iodine atoms, and to be connected to the *s* character of the C–X bond [8]; however, one can legitimately ask whether a single lighter atom like Br is sufficient to cause small but appreciable effects. A detailed investigation indicated that two effects are at work: typical DFT methods are not entirely adequate to model the correlation effects present in the system and, as surmised, relativistic effects. Thus, a combination

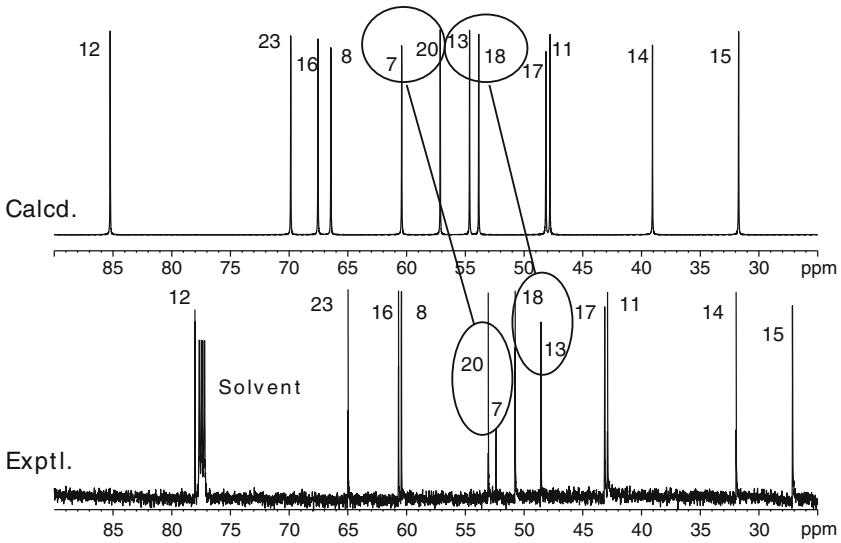

Fig. 5 Calculated (B3LYP/cc-pVTZ//6-31G(d,p)) and experimental ^{13}C spectrum of strychnine (aliphatic region). Inversions between calculated and experimental resonances are highlighted. Reproduced with permission from Ref. [15]. © 2006 Wiley-VCH

of MP2 shieldings and spin–orbit shieldings (σ_{so}) was found to provide an almost correct ordering of the signals (C2 > C6 > C3 > C4 > C5 > C1). σ_{so} terms were computed by means of the Zero-Order Regular Approximation (ZORA) [9–14] and were found to be markedly different among the six carbons, with a (definitely non-negligible) maximum of 12 ppm for C1, 3 ppm for C2 and less than 0.5 ppm for the others.

It is then apparent that, with the exception of halogen-bonded carbon atoms, DFT calculations have the power to predict at least the major features that characterize NMR spectra of simple organic molecules. The next logical challenge was to deal with more complex species, as reported in the next section.

3 Predicting the NMR spectra of naturally occurring substances

In organic chemistry, one generally deals with molecules having a spectacular variety of structures despite the relatively small number of atoms that make them up; this is somewhat at variance with inorganic chemistry, where structural variety is achieved through the presence of a variety of different constituent atoms—which has important implications for these studies, as described further down.

Tens of millions of organic molecules can be made or envisioned with just C, H, O, N as "building blocks". From an NMR viewpoint, this has relevant consequences. For one thing, by just ^{1}H and ^{13}C NMR even the most complex organic molecules can be investigated. More importantly, complexity translates into NMR spectra that exhibit a large number of closely spaced and variously coupled signals.

Ultimately, an NMR spectroscopist will aim at assigning each and every signal to hydrogen and carbon atoms, plus the connectivities among them—all this looking at peaks that may differ by as little as 0.01 ppm! Clearly, the challenge for DFT calculations becomes much more stringent; in particular, reliance on statistical parameters, such as those of Figs. 2 and 3 becomes questionable, since there is no guarantee that a given method will provide the right answers for the case in point. Consequently, we elected to evaluate all methods on a case-by-case basis, as shown subsequently.

3.1 Strychnine: the benchmark

The natural alkaloid strychnine has always been popular in the NMR community as a work bench for testing new pulse sequences, since its ^{1}H and ^{13}C spectra are sufficiently complex as to provide challenges in performance, at the same time being well understood. Strychnine was, therefore, a natural starting point for a computational approach, also because it is fairly rigid and weakly polar [15].

Let us first discuss the general trends reported in Fig. 3a–c. The slope values close to unity and the intercepts close to zero, joined with high correlation coefficients, do indicate a high predictive power of DFT calculations. Quite clearly, it would be easy to tell the values for different functional groups, and hence make such assignments. However, in typical situations this is rarely required; one would rather be interested in sorting out the crowded region of signals in the aliphatic region of, e.g. Fig. 3a. In this respect, the high statistical accuracy just noted may just not be sufficient, in the sense that statistical errors may exceed the minimum $\Delta\delta$ to be assigned. In fact, whenever two adjacent data

points in the plots of Fig. 3a and b are connected by a segment with negative slope, the two NMR signals would get a wrong assignment from calculation.

Thus, the most informative way to present the results is in the form of simulated spectra of the type seen in Fig. 1; this is shown in Figs. 4 and 5 for the most crowded aliphatic region. The most important features that emerge are: (a) several pairs of signals are in an incorrect order (not surprisingly, this occurs mostly for ^{1}H). (b) These interchanges occur only for signals separated by no more than 0.1 ppm. (c) Calculated coupling constants are such that the visual appearance of multiplets is always recovered, except where the $\Delta\nu/J$ ratio is strongly altered.

3.2 Nimbosodione

As a further example of prediction of NMR spectra we report the computational study of 13-acetyl-12-hydroxy-podocarpa-8,11,13-triene-7-one (**1**). Compound **1** was originally claimed to be one of the three new diterpenoids isolated from the stem bark of *Azadirachta Indica*, and thus named nimbosodione [16]. The proposed structure of the (+) enantiomer is shown in Scheme 2. It was later shown by total synthesis that such structural assignment was incorrect [17,18].

In Table 1 we report the experimental ^{1}H and ^{13}C chemical shifts of nimbosodione with the original incorrect assignment of the resonances to structure **1**, and the results of our calculations for **1**. The structure of the molecule is fairly rigid since also the acetyl group, in apolar solvents like chloroform, is likely to be involved in an intramolecular hydrogen bond.

Concerning ^{1}H resonances, the calculated chemical shift values of **1** appear to be not too far from the experimental resonances of nimbosodione, although the two aromatic protons (H11 and H14) and the acetyl protons are not in good agreement. In contrast, the calculated

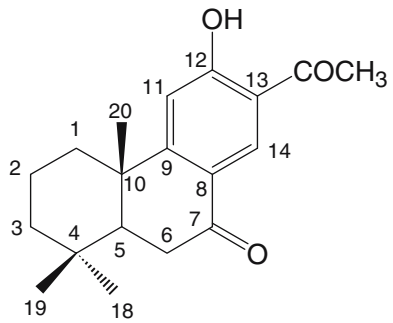

Scheme 2 Structural formula of (+)-13-acetyl-12-hydroxy-podocarpa−8,11,13-triene-7-one (**1**)

Table 1 Experimental ^{1}H and ^{13}C chemical shifts (ppm) of nimbosodione and calculated ^{1}H and ^{13}C chemical shifts of **1**

^{1}H	Exp	Calc	^{13}C	Exp	Calc
H1	1.61–1.70	1.54	C1	37.95	41.75
H1	2.54–2.58	2.31			
H2	1.61–1.70	1.68	C2	18.90	23.78
H2	1.94–1.99	1.89			
H3	1.42	1.31	C3	41.37	45.41
H3	1.52	1.50			
			C4	33.31	41.19
H5	1.83	1.73	C5	36.03	39.53
H6	2.69	2.65	C6	49.58	53.63
H6	2.58	2.52	C7	198.60	201.75
			C8	157.08	128.25
			C9	159.08	173.26
			C10	33.31	46.34
H11	6.72	6.96	C11	109.62	117.47
			C12	159.15	177.21
			C13	157.42	122.09
H14	7.82	8.93	C14	130.78	139.49
H18	0.92	0.92	C18	15.10	34.35
H19	0.97	1.02	C19	23.22	23.06
H20	1.20	1.24	C20	21.31	25.07
$COCH_3$	2.22	2.64	$CO\underline{C}H_3$	32.59	28.07
			$\underline{C}OCH_3$	198.62	212.84

Experimental data from Ref. [16] in $CDCl_3$; calculated values in the gas phase

^{13}C chemical shifts are significantly different from the experimental data. In particular, in the experimental spectrum of nimbosodione there are four carbon resonances, originally assigned to the aromatic quaternary carbons C8, C9, C12 and C13, which fall within a narrow range of about 2 ppm (see Table 1). The corresponding calculated chemical shifts of **1** are, instead, spread over a much wider range of about 55 ppm. Less dramatic differences can also be observed in the chemical shifts of the two carbonyl carbons, C7 and $\underline{C}OCH_3$: while in the experimental spectrum of nimbosodione both signals occur at 198.6 ppm, the calculated C7 and $\underline{C}OCH_3$ resonances of **1** are separated by about 10 ppm. The experimental ^{1}H spectrum of **1** has not been fully assigned since there are several resonances appearing as unresolved multiplets [17]. However, among the few proton resonances that have been assigned there are those of H11 (δ 6.96), H14 (δ 8.53) and of the acetyl protons (δ 2.70) [17]. These are in better agreement with the calculations than those of nimbosodione. The experimental ^{13}C spectrum reported in [18] has also not been assigned; therefore, it is again not possible to make a direct comparison with our calculated values. However, in contrast with the experimental spectrum of nimbosodione, the two most deshielded carbons, presumably C7 and $\underline{C}OCH_3$, are well separated and resonate at δ 197.04 and δ 204.42 [18]. In addition to this, and in agreement with the results of the calculation, the four

quaternary carbons C8, C9, C12 and C13 do not resonate so close to each other as in the experimental spectrum of nimbosodione.

The message is, then, that DFT calculations (especially of *J*-couplings) can capture the essential features of complex NMR spectra and can greatly help in the structural elucidation of newly isolated molecules, allowing to discard wrong structures whose calculated NMR spectra do not match the experimental one. It should be mentioned that similar approaches have been adopted also by Bifulco and coworkers to related issues in the natural-substances domain [19–23].

4 Calculated coupling constants in conformational analysis

A field where NMR *J*-couplings have always been a fundamental source of information is conformational analysis, owing mainly to the well-established Karplus relationship linking a vicinal ^3J(H,H) coupling to the H–C–C–H dihedral angle. There are, however, instances where such couplings cannot be accurately determined. One such case is that of bicyclic benzo-fused bicylic oxazines of the type sketched in Scheme 3. These compounds can exist in two conformations resulting in different dihedral angles between H-4a and H-4eq or H-4ax; however, interconversion between the two forms is fast even at very low temperatures, so that the coupling constants cannot be reliably extracted and one observes at best a population-weighted average. This is a typical playground for computational chemistry; indeed, after a prior calibration with one example where the exchange can be frozen, we were able to assign conformer populations through the calculation of relevant couplings; the level of accuracy is portrayed in Scheme 3 [24].

A similar approach was pursued to probe the conformational equilibria of phosphorus-containing heterocycles by means of *J*(P,H) couplings, after assessing the relative contributions of the various terms [25].

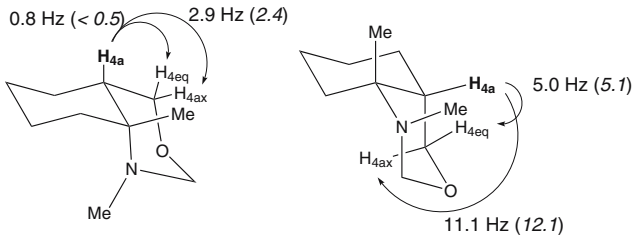

Scheme 3 Calculated *J*(H,H) coupling constants of *N*-in and *N*-out conformers of benzo-fused oxazines (experimental values in parenthesis). Data from Ref. [24]

5 NMR of heavy-atom nuclei

Computational studies involving heavy elements have always lagged behind in development with respect to molecules containing only light elements. There are several good reasons for this: these systems obviously have a large number of electrons, occupying shells with high angular momentum (such as *f* orbitals); electrons in inner shells are subject to large relativistic effects that ultimately have an influence on all molecular orbitals [26]. Furthermore, many such species, notably those based on transition-metal elements, exhibit a complex electronic structure with several closely spaced energy levels. It is not too surprising, therefore, that they are computationally challenging.

With regard to NMR properties, things are even worse: a popular workaround to some of the previous problems has been to adopt effective-core potential basis sets (ECP), where inner-core electrons are modeled in a simplified way, consistently with the notion that such electrons hardly participate in chemical bonding or reactivity [26]. This approach is hardly applicable for the calculation of properties that concern the behavior of the electron density in the vicinity of the nucleus, because ECPs do not have the correct form there. Even though shielding calculations with ECPs have been shown to have some predictive power [27,28], the approach as a whole is questionable.

So much for the bad news. The good news is that, very often, heteronuclear magnetic resonance works on species that contain just one or very few such atoms, e.g. where a metal center is complexed by organic ligands. Even more importantly, heavy-atom nuclei resonate in a far wider interval than light ones; chemical shift ranges of 10^3 ppm are common [29]. As a result, the requirements placed on computed results are often milder, since the resolving power required is lower (this is not always the case, as will be shown later).

The requirement of being able to deal with heavy atoms in a comprehensive manner, i.e. that takes into account the large number of electrons, relativistic effects thereon and accurate description of core shells, has been largely met by the Amsterdam Density Functional (ADF) code [30], where a consistent implementation of DFT with Slater (rather than Gaussian) basis sets and the ZORA formalism allows for a meaningful and informative computation of shieldings and couplings even for atoms as heavy as tungsten, mercury or lead [31,32]. Our own contributions to the field are described subsequently (in increasing atomic number).

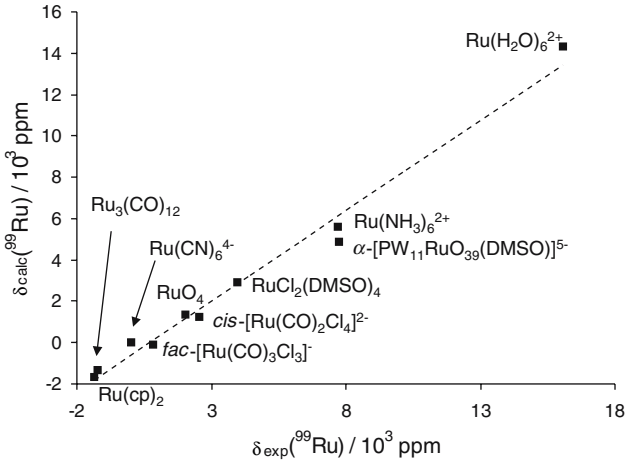

Fig. 6 Experimental and calculated (BP-ZORA/TZP) ^{99}Ru chemical shifts. The complexes reported encompass the whole 18,000-ppm range; a large number of tris(bipyridyl) complexes is known which resonate in the 7,000-ppm region. At both the scalar and spin–orbit levels the fit parameters are: $a = 1.0, b = -300$ ppm, $r^2 = 0.95$. Data from Ref. [34]

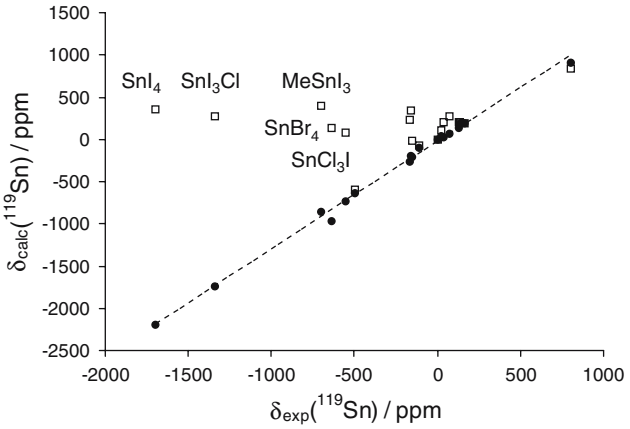

Fig. 7 Experimental and calculated (BP-ZORA/TZ2P) ^{119}Sn chemical shifts. *Filled circles* ZORA spin–orbit with correlation line; fit parameters are: $a = 1.3, b = -23$ ppm, $r^2 = 0.995$. *Empty squares* ZORA scalar for tin heavy halides (see text). Data from Ref. [39]

5.1 Ruthenium-99

Owing to its high quadrupole moment and low magnetogyric ratio [29,33], ^{99}Ru is a very difficult nucleus for NMR, to the point that experimental data are available for only a dozen species or so, and all this despite the great importance that ruthenium complexes have. With its 18,000-ppm range ^{99}Ru NMR offers a potentially useful avenue for the investigation of the numerous Ru complexes that find application in all areas of chemistry, especially synthesis and catalysis.

By employing the ADF scheme we were able to model all ^{99}Ru chemical shifts at a relativistic level, [34] remedying the deficiencies previously noted if the calculations were performed by the ECP method and conventional Gaussian basis sets [28] (Fig. 6). We also obtained a satisfactory accuracy for the ruthenium shielding in the polyoxometalate α-$[PW_{11}RuO_{39}(DMSO)]^{5-}$ [35].

5.2 Rhodium-103

Rhodium, apart from its known applications in catalysis, has recently gained novel popularity because of the possibility to build nanoscopic circuits based on binuclear complexes [36]. ^{103}Rh($I = {}^1/_2$) NMR [29,33] is of course a useful probe of the molecular geometry and electronic structure of such complexes. Therefore, a computational study of ^{103}Rh chemical shifts was performed at the ZORA relativistic DFT level [37]. The correlation between the calculated and experimental values for a set of mononuclear benchmark compounds and larger binuclear complexes was very satisfactory, provided that spin–orbit coupling was taken into account when heavy atoms (typically Br and I) were bound to Rh; then we proceeded to evaluate the influence of the electronic structure of the complex on ^{103}Rh shieldings [37]. The effect of changing the ancillary ligands was also correctly reproduced by the calculations.

5.3 Tin-119

Tin is a very important element in many areas such as industry, agriculture and biology [38], and a large quantity of tin NMR data, mainly related to ^{119}Sn, is available. In contrast, the investigation of tin NMR by quantum chemical methods is still at an early stage. Therefore we selected a set of tin(IV) compounds, including tin halides, for a systematic prediction of ^{119}Sn NMR properties [39]. The availability of several data pertaining to tin halides where Sn is bonded to one or more heavy halogens (Cl, Br, I) provided a further opportunity to test for the influence of relativistic spin–orbit effects on the shielding and couplings of ^{119}Sn. Indeed, the ZORA spin–orbit level is necessary to obtain a good agreement with experimental data even with chlorides, and is absolutely essential to get meaningful results in the case of bromides and iodides, as shown in Fig. 7. Spin–orbit coupling is essential also to correctly predict the coupling constants with heavy halogens, like Br or I.

Despite the general success of relativistic DFT methods, we also pointed out the limits of the protocol when small couplings $J(^{119}\text{Sn}, ^{13}\text{C})$ and $J(^{119}\text{Sn}, ^{1}\text{H})$ in similar alkyltin derivatives were sought [39]. Another application of computed ^{119}Sn NMR properties was the

structural characterization of a new ribonic acid derivative of Sn(IV) [40].

5.4 Xenon-129

Natural xenon contains 26% of the ^{129}Xe isotope, which has $I = 1/2$ and hence gives rise to sharp NMR lines with good sensitivity. Xenon NMR is acquiring more and more importance not so much in connection with its compounds, which are few and unstable, but because elemental xenon can be used as a molecular probe of weak interactions, owing to the great sensitivity of ^{129}Xe chemical shifts to even minute changes in the environment. Thus, it is of major interest to model the changes that occur in its NMR properties when a Xe atom approaches a molecule, membrane or solid surface. Since these changes are expected to be small, as a preliminary step we validated the methodology by looking at the few covalent Xe compounds [41].

The relevant results are shown in Fig. 8. It is immediately apparent that the correlation is generally good, but there are outstanding deviations that clearly deserve attention, most notably that for "XeF^+". Until a few years ago, the blame for this poor performance would have been placed entirely on the computational end. But we are now in a position to legitimately question the experimental results. Indeed, looking at the "small print" in the original report, we discovered that for the species generated in superacids the Authors postulated the XeF^+ or the bridged $[F–Xe–F–Xe–F]^+$ structure. Running the calculations on $Xe_2F_3^+$ resulted in quite a good agreement; thus strongly supporting the bridged species.

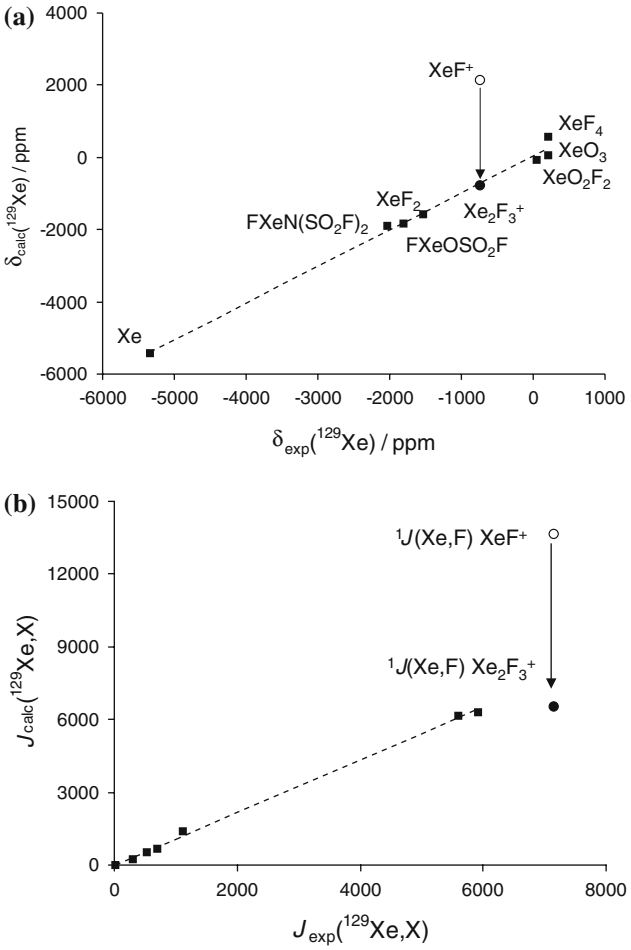

Fig. 8 Experimental and calculated (BP-ZORA scalar/TZ2P) ^{129}Xe chemical shifts and coupling constants. **a** Chemical shifts. Fit parameters of $\delta_{calc} = a\delta_{exp} + b : a = 1.01, b = 28\,\text{ppm}, r^2 = 0.993$. **b** Coupling constants. Fit parameters (excluding XeF^+) of $J_{calc} = aJ_{exp} + b : a = 1.09, b = 17\,\text{Hz}, r^2 = 0.999$. The *arrows* highlight the different NMR parameters of XeF^+ and $Xe_2F_3^+$. Data from Ref. [41]

5.5 Tantalum-181

The ^{181}Ta nucleus belongs to the fairly large group of elements which possess NMR-active isotopes but are hardly studied, owing to major difficulties in detecting their broad and/or weak signals (like, e.g. ^{33}S, ^{47,49}Ti, ^{57}Fe, ^{187}Re, ^{187,189}Os and ^{193}Ir) [33]. As a consequence, a potentially useful probe in certain areas of chemistry falls into oblivion. Obviously, the capability to predict the location of a given NMR signal, even with relatively low accuracy, would be helpful. The following example tries to make this point by looking at ^{181}Ta chemical shifts for the few experimentally studied species (Table 2; Fig. 9). The accuracy is limited by that of experimental data (lines are several kHz broad), and again the correlation has an adequate predictive value.

5.6 Tungsten-183

Tungsten has only one NMR-active isotope, ^{183}W($I = 1/2$) [29,33]. Albeit endowed with a fair abundance of 14%, its very small magnetogyric ratio makes it a difficult nucleus for NMR. There are, however, major reasons to encourage such studies: ^{183}W signals are sharp and hence provide high resolution; most importantly, many tungsten complexes are crucially important in catalysis. Most such compounds belong to the numerous and varied family of polyoxometalates (POM), and it is in this area that we have focused our efforts (see e.g. Fig. 10).

As before, we firstly approached the problem analyzing mononuclear complexes by means of ECP basis

Table 2 Experimental and calculated ^{181}Ta chemical shifts

	Exp	σ_p	σ_d	σ_{SO}	σ	δ
TaS_4^{3-}	445	−9662.55	8453.65	1765.768	556.866	2030.49
$TaSe_4^{3-}$	1435	−10691.60	8448.71	1764.115	−478.776	3066.14
$TaTe_4^{3-}$	3525	−12549.52	8457.87	1962.23	−2129.42	4716.78
$TaCl_6^-$	0	−7805.27	8458.26	1934.364	2587.361	0
$Ta(CO)_6^-$	−3450	−3575.54	8463.21	2047.435	6935.104	−4347.74
TaF_6^-	−2295	−5557.18	8445.76	1959.24	4847.82	−2260.46
TaF_7^{2-}	[a]	−5482.53	8448.25	1975.71	4941.43	−2354.07

^{181}Ta chemical shifts at the BP-ZORA spin–orbit/TZP level. Experimental data cited in Ref. [33]
[a]Note that the ambiguous assignment of the signal attributed to TaF_6^- would not be addressed by ^{181}Ta NMR, since the alternative proposal TaF_7^{2-} has a virtually identical chemical shift

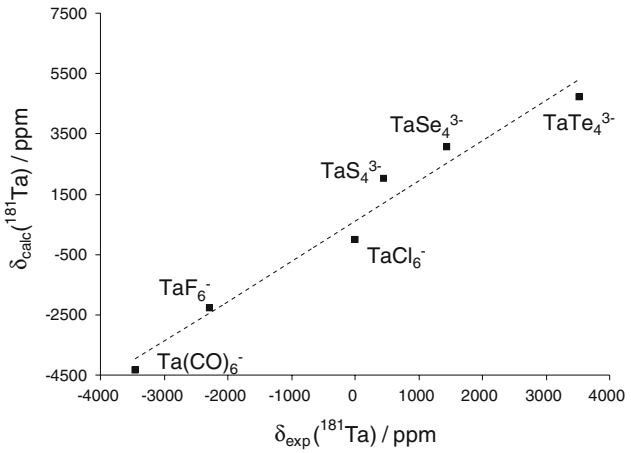

Fig. 9 Experimental and calculated ^{181}Ta chemical shifts (BP-ZORA spin–orbit/TZP). Fit parameters of $\delta_{calc} = a\delta_{exp} + b : a = 1.3, b = 609\,\text{ppm}, r^2 = 0.97$

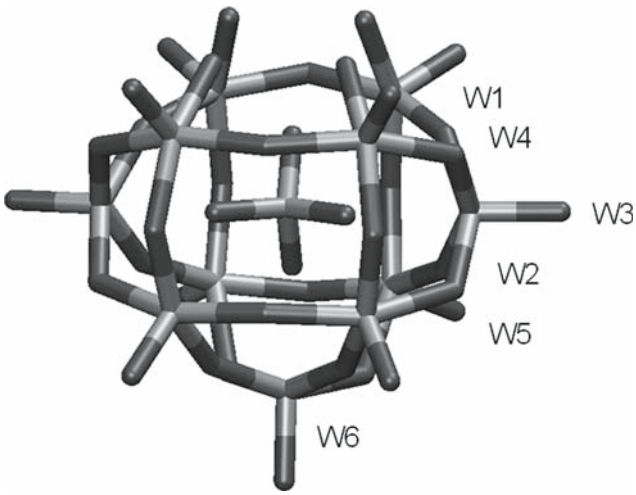

Fig. 10 Structure and numbering of the Keggin polyoxometalate $\alpha - [PW_{11}O_{39}]^{7-}$ with C_s symmetry. The 11 tungsten atoms give rise to a 2:2:2:2:2:1 spin system, with one unique signal arising from W6 lying in the symmetry plane

sets [27] and later by relativistic ZORA methods [42], obtaining results of similar quality as those earlier seen.

In the context of POM chemistry, however, important challenges lay ahead. Most POMs feature a number of W(VI) atoms (5–30 and more) lying in slightly different environments, with correspondingly similar chemical shifts: the range of 8,000 ppm is thus reduced to some 300–500 ppm, and often much less.

The situation is even more complicated because these species are negatively charged, and their spectra are generally obtained in polar solvents, which brings in issues like the effects of counterion and solvent. In a preliminary wide-range study, we examined a few representative cases [42]. For example, the ^{183}W spectrum of $\alpha - [PW_{11}O_{39}]^{7-}$ features six signals in the 2:2:2:2:2:1 ratio, lying within just 50 ppm in an order that depends on the counterion. We then found that the ordering of the signals was mostly incorrect if one took the isolated ion into account; conversely, if a $Li(H_2O)^+$ counterion was assumed to lie in the upper cavity defined by the four W1 and W4 atoms (the "lacuna"), the resulting order was profoundly affected, leading to a better agreement with experiment. A following study highlighted the necessity of including solvent effects both in the geometry optimization and in the shielding calculation, and of running the calculations at the ZORA spin–orbit level [43].

A further important issue connected with the NMR of POMs concerns vicinal spin–spin couplings of the type $^2J_{WW}$. All POMs contain a large number of W–O–W units which give rise to sizable couplings. Owing to the caged structure of POMs, the W–O–W angle α cannot take arbitrary values, but is rather constrained to two ranges with α of approximately 130° (edge-sharing) or 150° (corner-sharing). The magnitude of $^2J_{WW}$ depends strongly on α, with values of 5–12 Hz or 15–30 Hz, respectively. Thus, these coupling constants find extensive application in the structure determination of

POMs. Nonetheless, cases are known where this empirical rule is apparently violated. For example, in the case of $\gamma-[SiW_{10}O_{36}]^{8-}$ one such coupling (of the corner-sharing type) is only 4.9 Hz even though the W–O–W angle would require a value in the high range. Clearly, the occurrence of such exceptions called for a non-empirical validation of the empirical rule. We approached the problem by firstly analyzing in detail a basic POM fragment, $[W_2O_9]^{6-}$, for which we could determine the coupling surface as a function of α and r_{WO} (Scheme 4). By this, we established that (a) the angular dependence indeed conforms to the empirical rule; (b) there is, in addition, a strong distance dependence that cannot be overlooked. Most importantly, (c) accurate couplings can be computed with a locally dense basis set in which only the three involved atoms (W–O–W) are treated at a high level. This recognition allowed us to calculate the couplings in $\gamma-[SiW_{10}O_{36}]^{8-}$, thereby demonstrating that the small value of $^2J_{WW}$ (4.9 Hz) can be successfully reproduced (5.8 Hz), and that it is entirely due to an exceptionally long r_{WO} distance [44].

5.7 Mercury-199

^{199}Hg, having $I = 1/2$, gives rise to well-resolved NMR spectra and is often employed in structural studies of mercury compounds [29]. For these reasons, ^{199}Hg has been used to benchmark the performance of relativistic methods in the calculation of nuclear shieldings [5]. A peculiarity that renders ^{199}Hg NMR really conspicuous is the size of its homonuclear coupling constants, which reach the highest values known; the computed ^1J(Hg,Hg) in the naked Hg_2^{2+} cation is not less than 800–900 kHz [45]. The experimental value of "just" 284.1 kHz [46] refers to crown–ether complexes, which could also be successfully modeled as 278.4 kHz by Autschbach and Ziegler [45]. Analogously, the Hg_3^{2+} cation complexed with solvent or counterions yielded a ^1J(Hg,Hg) of 100–140 kHz [45] against an experimental value of 139.6 kHz [47].

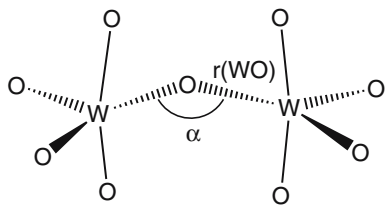

Scheme 4 The $[W_2O_9]^{6-}$ fragment used as a model of POMs. Values of $^2J_{WW}$ have been computed covering the relevant part of the (α, r_{WO}) surface

Table 3 Calculated coupling constants in the Hg_4^{2+} cation

Coupling constant	PSO (Hz)	FC + SD (kHz)	Total (kHz)
^1J(Hg1,Hg2)	−1860	34.5	32.7
^1J(Hg2,Hg3)	−377.1	100.0	99.6
^2J (Hg1,Hg3)	−0.5	149.8	149.8
^3J (Hg1,Hg4)	−29.4	178.0	178.0

At the BP-ZORA spin–orbit/TZ2P level, for ^{199}Hg, DSO terms are always smaller than 0.1 Hz. In the ZORA formalism at the SO level the PSO and FC + SD contributions contain cross terms with each other

We built on those results, firstly extending the study to the Hg_4^{2+} cation (C_{2h}) [47]. The structure was optimized at the BP-ZORA scalar/TZP level; numbering the spin system as Hg(1)–Hg(2)–Hg(3)–Hg(4), we calculated bond lengths as $r_{12} = 2.769$ Å, $r_{23} = 2.723$ Å and a Hg(1)–Hg(2)–Hg(3) bond angle of 178.9°. These values can be compared to the respective experimental X-ray data of 2.620 and 2.588 Å, 177.27° [48]. Its couplings are still in the kHz range, and the one-bond couplings in $[Hg(1)–Hg(2)–Hg(3)–Hg(4)]^{2+}$ are all smaller than two- and three-bond ones (Table 3) [45]. Unfortunately, this species is insufficiently stable in solution to allow for an experimental verification.

A further point of interest concerns the so-called "grid compounds" extensively studied by Lehn, which self-assemble to form extended networks containing metal centers (including Hg(II)) at regular positions in a grid ([49] and references therein). These complexes have been proposed as systems to store/retrieve information, and J-coupling is one means to achieve this. Again, computational chemistry can help designing systems where desirable characteristics can be predicted or enhanced. Owing to the size of these systems, we had to design a simplified model which could however capture the essentials of the system. Thus, we computed mercury coupling constants in the complex depicted in Fig. 11, which gives rise to a simple 2 × 2 rectangular grid.

The structure of Fig. 11 (148 atoms, no symmetry) was optimized at the BP-ZORA scalar level, with the TZP basis set for Hg (4f shell frozen, Hg4f.TZP), DZP for C and N (1s shell frozen, C1s.DZP, N1s.DZP), and DZP for H. The use of frozen-core basis sets, in which the orbitals designated as atomic cores (e.g. up to the 4 f shell for Hg) are not optimized in the SCF procedure, was mandated by the large size of this system. The coupling calculation was then run on the optimized structure, employing an all-electron basis set for Hg (TZ2P) and keeping the basis for the other atoms at the DZP, frozen-core level. The scalar ZORA method was used,

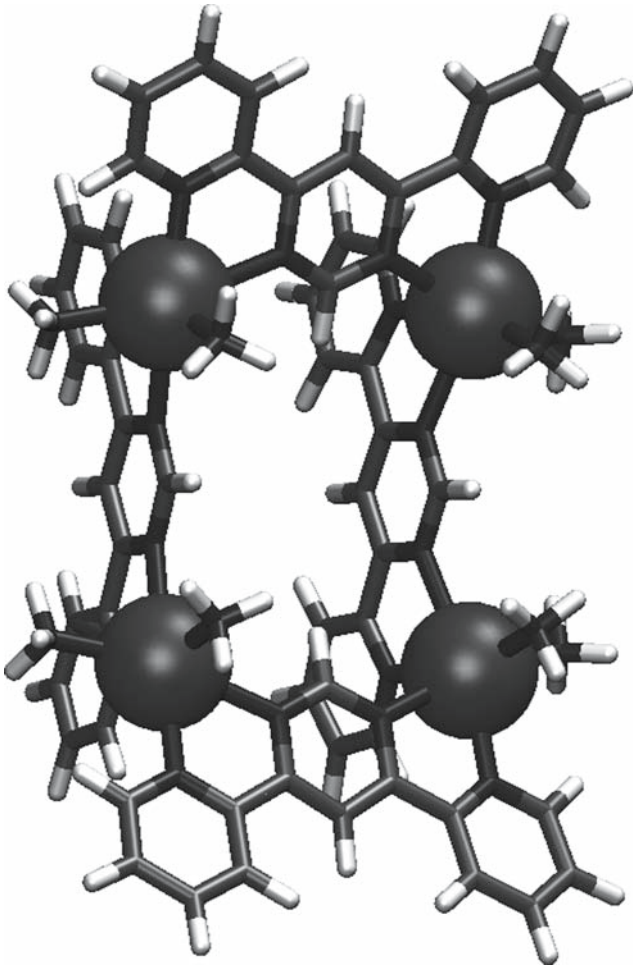

Fig. 11 A model Hg(II) complex inspired by Lehn's "grid compounds". The four mercury atoms define a rectangle with ca. 7 Å side

Table 4 Calculated coupling constants in a Lehn's "grid compound"

Coupling constant	DSO	PSO	FC	Total
J(Hg1,Hg2) (horizontal)	0.06	0.04	−36.4	−36.3
J(Hg1,Hg3) (vertical)	0.01	0.05	−17.9	−17.9
J(Hg1,Hg4) (diagonal)	0.00	0.00	0.1	0.1

In Hertz at the BP-ZORA scalar level, for ^{199}Hg, see text for basis sets

and the calculation was restricted to the DSO, PSO and FC terms only. The results are collected in Table 4.

The coupling constant between two ^{199}Hg nuclei across the "horizontal side" (Hg1–Hg2, 7.088 Å) was a sizable −36 Hz, the one across the "vertical side" (Hg1–Hg3, 7.196 Å) was −18 Hz, and only 0.1 Hz across the diagonal (Hg2–Hg3, 10.101 Å). In contrast, in a rectangle of four naked mercury ions placed in the same relative positions no coupling is calculated. One then sees that the ligands are essential for this very long-range coupling (these would be ^{10}J if this terminology makes sense at all here). These results highlight again the extremely strong spin–spin coupling that mercury nuclei can exhibit even when separated by large distances, and may suggest ways to achieve the desired effect of transmitting or storing information.

6 Through-HB spin–spin coupling

Spin–spin coupling is commonly thought of as the hallmark of covalent bonding; this concept is even built into the ^{n}J notation, where n stands for the number of bonds intervening between the two coupled nuclei. In organic chemistry this notion is rooted in the well-known fact that most such couplings rapidly fall off when n exceeds 5–6. Thus, the finding that in hydrogen-bonded species involving HF and F^- at low temperatures there was a coupling as large as 100 Hz was something of a surprise [50]. Despite the obvious fundamental implications, these findings remained some of a curiosity (together with certain unusually large long-range couplings involving ^{19}F) until similar couplings were demonstrated to exist between nuclei involved in much weaker and much more important hydrogen bonds (HB), like those of nucleic acids and peptides (Scheme 5).

The existence of a coupling previously thought to be unmeasurably small spawned much interest in the biomolecular NMR community, since a new conformational constraint could be employed to probe the spatial proximity of specific atoms. Thus, together with the deployment of new experimental techniques, fundamental questions arose, like: (a) What structural features of the HB (distance, angle, dihedral angle) determine the magnitude of J? (b) Is there a relationship between the HB strength and J? (c) What range of J values can be expected for a given system?

Work from this laboratory [51] provided a first comprehensive set of answers. Firstly, a model system made of two formamide molecules was investigated: this system (Scheme 6) was sufficiently small as to allow a detailed mapping of the $^{3h}J_{NC'}$ coupling surface as a function of the most relevant geometrical parameters (r, ψ). Only the Fermi-contact term was computed at the B3LYP/6-31G(d,p) level.

The main conclusions thus drawn on the magnitude of $^{3h}J'_{NC}$ were: (a) A marked distance dependence, especially for $\psi = 180°$; (b) No relationship between the magnitude of J and linearity of HB; (c) No dependence on the dihedral angle between the planes defined by each amide molecule. Furthermore, the correct order of magnitude (between −0.2 and −1.7 Hz) was predicted,

Scheme 5 Spin–Spin coupling through hydrogen bonds. *Left to right* $^{19}F–H\cdots{}^{19}F^-$ in liquid HF at low temperatures, $^{15}N–H\cdots{}^{15}N$ in nucleic-acid base pairs, $^{15}N–H\cdots O={}^{13}C$ in peptides. The *superscript* "h" denotes through-HB coupling

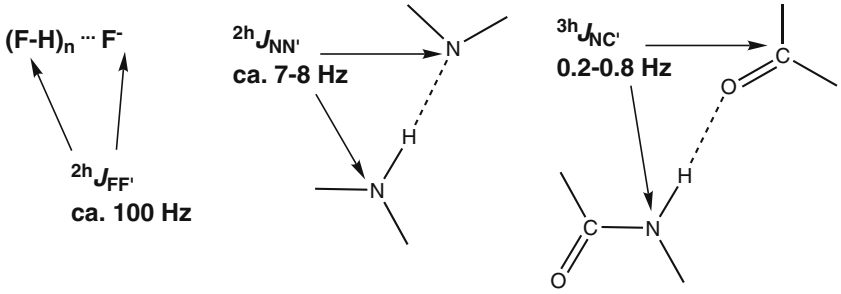

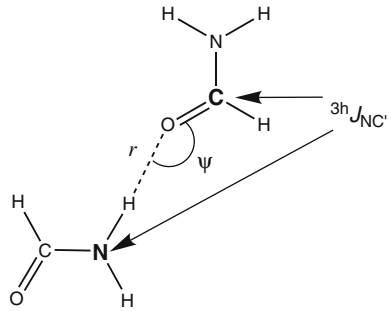

Scheme 6 The formamide hydrogen-bonded dimer as model system

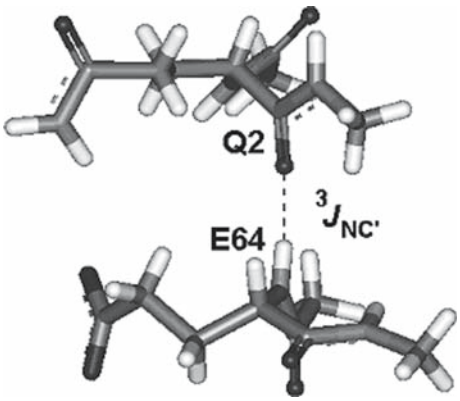

Fig. 12 Spatial arragement of the Glu-64 (donor)–Gln-2 (acceptor) pair in ubiquitin

in agreement with the few then available experimental values, for arrangements leading to a stable HB, with a maximum for $\psi = 150°$. The lack of influence from the dihedral angle was tentatively traced to the σ symmetry of the molecular orbitals that connect the two interacting molecules.

These results were used as reference to investigate the through-HB coupling in the then only available data set (ubiquitin). Amino acid pairs for which a through-HB coupling had been ascertained were cut from the structure of ubiquitin, and left in their native relative arrangement (see e.g. the Glu-64–Gln-2 pair in Fig. 12, for which a value of 0.8 Hz had been determined). In most cases the correct magnitude could be predicted.

7 Through-space spin–spin coupling

We have seen in the previous section that spin–spin coupling does not strictly require the existence of a covalent bond between the involved nuclei, even though the notion of some extent of bonding is firmly rooted in our concept of hydrogen bonding. This novel perception brought a new awareness which naturally led to the next logical question, can there be a spin–spin coupling *without* a covalent bond? There is an obvious stumbling block in demonstrating this proposition—all non-bonded molecular pairs will, by necessity, be very short-lived and this will inevitably clash with the long timescale of NMR spectroscopy. There is no such difficulty in the computational approach, so this topic perfectly suits the purpose of this investigation. It is useful to recall at this stage that, without a recognizable covalent or even hydrogen bond in between, any predicted coupling might be hailed as "through space", and will be labeled accordingly.

Indeed, early reports were discouraging, since in $Xe\cdots Xe$ and $Xe\cdots H$ calculated coupling constants were much below 10^{-3} Hz [52]. A perspective shift was provided by Pecul, who calculated a stunning 1.3-Hz coupling between two ^{3}He nuclei in He_2, a system for which no one would admit any degree of chemical bonding [53]. Interesting as it was, however, this result did not go beyond a proof of principle; there is no chemically interesting system where this result might be put to advantage. There are, however, several other weakly bound systems which are important in various areas of chemistry, to which we turned our attention as described hereafter.

7.1 Through-space coupling in CH–π complexes

Among weak nonbonding interactions the so-called CH–π interaction, where a C–H bond acts as "donor" towards an aromatic π system as "acceptor", plays an

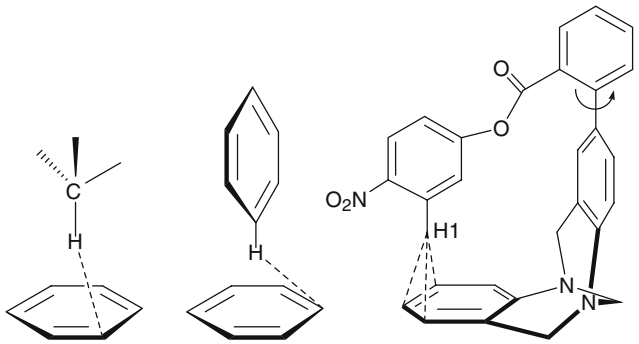

Fig. 13 CH–π systems investigated. *Left to right* $CH_4 \cdots C_6H_6$, $(C_6H_6)_2$, Wilcox balance. For these systems, the "through-space" couplings are negligible for protons, and take values of 0.1–0.3 Hz for the ^1H, ^{13}C couplings indicated

established role in dictating the structure and stability of many organic systems [54]. Most such systems, however, still share the unwanted feature of being too labile to be amenable to NMR studies: thus, even if one were able to measure predictably small coupling constants, the observable value would be a weighted average involving a large fraction of unbonded partners, where no coupling would exist. Despite these major obstacles and the lack of experimental data, however, we deemed the topic intriguing enough to warrant a detailed theoretical investigation. Initially, we employed DFT methods to probe simple "van der Waals molecules" arranged as required for a CH–π interaction, like $CH_4 \cdots C_6H_6$ or $(C_6H_6)_2$ [55], proceeding with the use of accurate ab initio methods [56]. Both approaches concurred in predicting (at equilibrium distance) negligible couplings between protons and small but consistently non-negligible ones (0.1–0.3 Hz) between the proton in the donor and a ^{13}C in the aromatic acceptor (Fig. 13). Other features were also probed [57,58]. Most importantly, we pinpointed a few cases drawn from supramolecular chemistry where certain molecular moieties were arranged as in model systems, like an acetonitrile–calix[4]arene complex and the "Wilcox balance", where we found again similar trends [55,56].

To date, there have been no experimental determinations related to these predictions. Nonetheless, we deemed it interesting to further probe this issue, moving on to through-space couplings involving elemental xenon.

7.2 Through-space coupling involving elemental xenon

As mentioned before, ^{129}Xe is a favorable nucleus for NMR. Xenon NMR has acquired an outstanding role owing to the extreme sensitivity of the Xe atom to even small changes in its environment, which can be monitored through ^{129}Xe NMR. These properties, joined to its chemical and biological inertness, make it an ideal NMR probe for weak interactions. The scenario is made even more favorable because the spin polarized state of ^{129}Xe can be populated by laser irradiation to an extent much higher than the thermal population (hyperpolarization); taking advantage of the extremely slow relaxation, one can measure very strong signals. Lately, therefore, the chemical shift and relaxation rate of Xe are finding use in MRI for materials science and medicine.

On the other hand, one should also recall that spin–spin coupling involving heavy atoms tends to reach high values, as shown before for Hg. From this standpoint it seemed worthwhile to investigate through-space couplings between Xe and nuclei in small molecules taken as models of the weak interactions that one expects when xenon interacts with organic materials like membranes or living tissue (methane, benzene) or inorganic ones like zeolites (an $O[Si(OH)_3]_2$ fragment), see Scheme 7 [41]. Not too surprisingly, we found again that at distances where the interaction is stabilizing ^{129}Xe–^1H and ^{129}Xe–^{13}C coupling constants take non-negligible values of a few tenths of Hertz. Interestingly, the largest such coupling was predicted in system (c) between ^{129}Xe and ^{17}O (ca. 4 Hz), but not with ^{29}Si.

As an extension to this work, we further calculated trends in the ^{129}Xe chemical shift with varying distance to the interacting partner, since these trends are useful in molecular dynamics simulations, with particular regard for a more realistic membrane model [58].

As remarked before, actually measuring these small couplings is a major challenge for experimental NMR. Xenon systems may have a greater chance of success, employing hyperpolarized Xe and SQUID-NMR detection as recently suggested [59].

In the following last section, we will present a peculiar case where through-space coupling has been experimentally detected. As such, it was a chance not to be missed.

7.3 Through-space coupling in thallium cryptates

Through-space coupling has been observed experimentally in the dithallium(I) cryptate shown in Fig. 14 [60]. The authors reported a $J(^{203,205}Tl, ^1H)$ of 17 Hz between the pair of equivalent Tl atoms and the aromatic proton of the bridging link, located at 3.816 Å from the metal ions. The authors also claimed that the $J(^{203,205}Tl, ^{203,205}Tl)$ should be much larger than 17 Hz despite the relatively large distance of 4.376 Å between the two ions [60].

We have investigated this system by relativistic DFT calculations. Since the size of the system is significant,

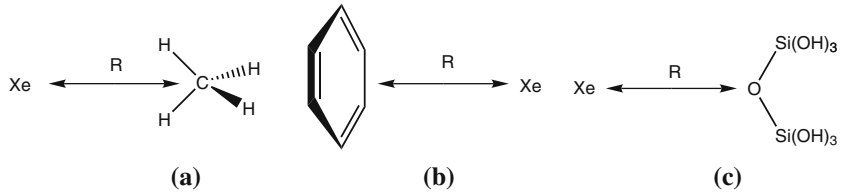

Scheme 7 Some of the model systems investigated which show through-space coupling between ^{129}Xe and ^{1}H, ^{13}C or ^{17}O. **a** Xe–methane; **b** Xe–benzene; **c** Xe–O[Si(OH)$_3$]$_2$. NMR properties were calculated as a function of the intermolecular separation R

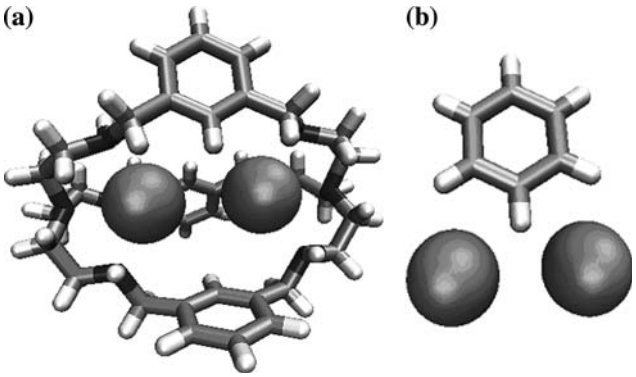

Fig. 14 3D structures of **a** the dithallium(I) cryptate system (X-ray structure from Ref. [60]) and **b** the model system

together with the X-ray structure of the full cryptate (Fig. 14a) we also devised a model system composed of the two Tl(I) ions and one benzene molecule in the same relative position as the benzene ring in the cryptate (Fig. 14b).

In Table 5 we report the calculated coupling constants for the model system. The magnitude of the calculated $J(^{205}\mathrm{Tl}, ^{1}\mathrm{H})$ between Tl(I) and the aromatic proton (ca. 15 Hz at all levels) is in good agreement with the experimental data. The results of our calculations seem to be converged with respect to the basis set size, as far as $J(^{205}\mathrm{Tl}, ^{1}\mathrm{H})$ is concerned, and the use of the more expensive TZ2P basis set is not necessary. Although the calculated values at the SC and SO level are quite similar, the various contributions are affected by the level of theory. The agreement we observe for the total J, therefore, stems from a compensation of errors. Concerning the $J(^{205}\mathrm{Tl}, ^{205}\mathrm{Tl})$ coupling constant, the values we obtain are indeed much larger than the proposed lower limit of 17 Hz [60]. However, widely different results are obtained according to the basis set and the relativistic level. For example, at variance with typical results, at the SO level the PSO contribution is the dominant term, but the other contributions are also strongly affected. Thus, we can only estimate a $J(^{205}\mathrm{Tl}, ^{205}\mathrm{Tl})$ coupling constant of ca. 2 kHz.

The size of the cryptate system sets stringent limits on the basis set quality and relativistic level. At the ZORA scalar level, we were able to adopt the TZP basis as before, but in the case of the computationally intensive spin–orbit one we had to resort to a locally dense basis set like in the case of tungsten couplings [44]. Thus, the atoms that had been included in the model system were assigned the TZP basis, whereas the remaining atoms were assigned a frozen-core basis set of DZP quality, C and N with the 1s shell frozen. These results are given in Table 6 and show a substantial agreement (although strictly they are not comparable owing to the difference in the basis set). In any case, we predict a through-space $J(^{205}\mathrm{Tl}, ^{1}\mathrm{H})$ of 35 Hz and a $J(^{205}\mathrm{Tl}, ^{205}\mathrm{Tl})$ of 55 kHz. All values turn out to be quite different from those of the model system; notably, the ^{205}Tl–^{205}Tl coupling is estimated one order of magnitude larger than in the model. Nevertheless, the calculated value for $J(^{205}\mathrm{Tl}, ^{1}\mathrm{H})$ still has the correct order of magnitude. Thus it is apparent that recourse to simplified models, as was successfully done with ^{183}W, may not always be warranted. This behavior resembles that of the grid compound of Table 4, where only the inclusion of all ligands resulted in a sizable coupling.

8 Outlook and perspectives

Computational NMR has evolved into a well-defined subdomain of computational chemistry. It is also becoming "mature" in the sense that one sees more and more often this approach being employed as part of a wider-range investigation (as opposed to validation or methodological studies). Like its experimental counterpart, it embraces all fields of chemistry and therefore its potential applications raise the interest of all researchers involved in NMR spectroscopy. Of course, there are still several challenges that have to be met before this approach becomes a standard tool in chemistry: some difficulties are inherent to the nature of the systems investigated (e.g. in the case of heavy atoms), others are rooted in the complex nature of the molecules of interest (as is often the case of organic species) and others still stem from the neglect, or incomplete accounting, of solvent effects. Eventually, the level of description of the (electronic) structure will have to move from a static picture, such as that commonly adopted, to a dynamic

Table 5 Calculated coupling constants involving ^{205}Tl in the model $Tl_2(C_6H_6)^{2+}$ system

$J(^{205}Tl,X)$ (Hz)								
Basis	Level	X	DSO	PSO	FC	SD	FC + SD[a]	Total
TZP	SC	^{205}Tl	0.0	350.2	6640.7	−126.9	6513.8	6864.1
		^{1}H	0.6	1.9	16.1	−3.9	12.2	14.7
	SO	^{205}Tl	0.0	−5041.5			1844.9	−3197.4
		^{1}H	0.6	7.9			7.1	15.5
TZ2P	SC	^{205}Tl	0.0	318.0	6479.0	−108.3	6370.7	6688.7
		^{1}H	0.6	1.6	16.0	−3.6	12.4	14.6
	SO	^{205}Tl	0.0	−4223.0			2478.6	−1744.4
		^{1}H	0.6	7.1			7.7	15.4

[a] In the ZORA formalism at the SO level the PSO and FC + SD contributions contain cross terms with each other

one that accounts for internal mobility, solvent effects and solvation dynamics at the same time. This is a currently active field of research (see e.g. [61]) that stretches computational facilities to their limits, and as such is still limited to relatively small systems.

A further goal is the computation of NMR spectra of paramagnetic substances [62]. Once considered to lie at the borders of the scope of NMR, it is now recognized that such spectra can often not only be obtained, but provide valuable information as well [63].

By accounting our recent work in this area we hope to have conveyed the usefulness and liveliness of the approach as a whole, thus attracting more active researchers into considering the calculation of NMR spectra as a worthwhile tool in the pursuit of their scientific goals.

9 Computational details

Calculations run for this work were performed with the Amsterdam Density Functional suite of programs (ADF) [30] or Gaussian 03 [64].

Gaussian 03 calculations on nimbosodione were carried out with the B3LYP hybrid functional [65,66] and the cc-pVTZ basis set, after geometry optimization at the B3LYP/6-31G(d,p) level.

In ADF calculations we employed the Becke88-Perdew 86 GGA functional [67,68]. Relativistic effects were dealt with by means of the Zero-Order Regular Approximation (ZORA) [9–14] in connection with specially optimized basis sets composed of Slater functions [30]. Double-zeta singly polarized, triple-zeta singly- and doubly-polarized basis sets are denoted as DZP, TZP and TZ2P, respectively as defined in the package. When required, frozen-core basis sets can be employed where the orbitals designated as atomic cores are not optimized in the SCF procedure; these basis sets are denoted as, e.g. Hg4f.TZP, where shells up to 4*f* are considered as core shells. ZORA calculations can include only scalar effects (SC) (the equivalents of Darwin and mass-velocity) or spin–orbit coupling as well (SO). The *nmr* and *cpl* property modules then allow for the calculation of these properties in a consistent way.

Table 6 Calculated coupling constants involving ^{205}Tl in the cryptate system

$J(^{205}Tl,X)$ (Hz)							
Basis	Level	X	DSO	PSO	FC	FC + SD	Total
TZP	SC	^{205}Tl	0.4	6.4	55769		55776
		^{1}H	1.1	−0.9	34.6		34.8
Mixed	SO	^{205}Tl	0.4	40.2		55520	55560
Basis set[a]		^{1}H	1.1	−0.7		34.2	34.6

[a] TZP for the atoms also included in the model system. DZP·1s for the remaining atoms

The structure of Hg_4^{2+} was optimized at the ZORA SC/TZP level under the constraints of C_{2h} symmetry. Coupling constants were then computed at the ZORA SO/TZ2P level. The structure of Fig. 11 was optimized at the ZORA SC level, with a locally dense basis set: Hg4f.TZP for Hg; C1s.DZP, N1s.DZP for C and N, and DZP for H. The use of frozen-core basis sets was mandated by the large size of this system.

For the model $Tl_2(C_6H_6)^{2+}$ system we ran calculations at the ZORA SC and SO levels, with TZP and TZ2P basis sets. For the full system we tested two levels of theory: the ZORA SC level, with the TZP basis set (at this level we have not included the Spin-Dipole term in the calculation of the coupling constants); the ZORA SO level, including all contributions to the coupling constants, with a mixed basis set: TZP for the atoms also included in the model system and DZP with the 1s shell frozen for the remaining atoms.

Acknowledgments This work was financially supported by the University of Padova (Progetto di Ricerca di Ateneo CPDA045589).

References

1. Bagno A, Rastrelli F, Saielli G (2005) Prog NMR Spectrosc 47:41
2. Bagno A, Scorrano G (2000) Acc Chem Res 33:609
3. Nicolaou KC, Snyder SA (2005) Angew Chem Int Ed 44:1012
4. Helgaker T, Jaszuński M, Ruud K (1999) Chem Rev 99:293
5. Kaupp M, Bühl M, Malkin VG (eds) (2004) Calculation of NMR and EPR parameters. Wiley-VCH, Weinheim
6. Bagno A (2001) Chem Eur J 7:1652
7. Bagno A, Rastrelli F, Saielli G (2003) J Phys Chem A 107:9964
8. Kaupp M, Malkina OL, Malkin VG, Pyykkö P (1998) Chem Eur J 4:118
9. Schreckenbach G, Ziegler T (1995) J Phys Chem 99:606
10. Schreckenbach G, Ziegler T (1997) Int J Quantum Chem 61:899
11. Wolff SK, Ziegler T (1998) J Phys Chem 109:895
12. Wolff SK, Ziegler T, van Lenthe E, Baerends EJ (1999) J Chem Phys 110:7689
13. Autschbach J, Ziegler T (2000) J Chem Phys 113:936
14. Autschbach J, Ziegler T (2000) J Chem Phys 113:9410
15. Bagno A, Rastrelli F, Saielli G (2006) Chem Eur J 12:5514
16. Ara I, Siddiqui BS, Faizi S, Siddiqui S (1990) J Nat Prod 53:816
17. Ghosh S, Ghatak UR (1992) J Chem Res 10:S352
18. Li AP, Bie PY, Peng XS, Wu TX, Pan XF, Chan ASC, Yang TK (2002) Synth Commun 32:605
19. Barone G, Gomez-Paloma L, Duca D, Silvestri A, Riccio R, Bifulco G (2002) Chem Eur J 8:3233
20. Barone G, Duca D, Silvestri A, Gomez-Paloma L, Riccio R, Bifulco G (2002) Chem Eur J 8:3240
21. Cimino P, Bifulco G, Evidente A, Abouzeid M, Riccio R, Gomez-Paloma L (2002) Org Lett 4:2779
22. Cimino P, Gomez-Paloma L, Duca D, Riccio R, Bifulco G (2004) Magn Reson Chem 42:S26
23. Bifulco G, Bassarello C, Riccio R, Gomez-Paloma L (2004) Org Lett 6:1025
24. Tähtinen P, Bagno A, Klika KD, Pihlaja K (2003) J Am Chem Soc 125:4609
25. Tähtinen P, Bagno A, Koch A, Pihlaja K (2004) Eur J Org Chem 4921
26. Jensen F (1999) Introduction to computational chemistry. Wiley, Chichester
27. Bagno A, Bonchio M (2000) Chem Phys Lett 317:123
28. Bagno A, Bonchio M (2002) Eur J Inorg Chem 1475
29. Mason J (ed) (1987) Multinuclear NMR. Plenum, New York
30. te Velde G, Bickelhaupt FM, Baerends EJ, Fonseca Guerra C, van Gisbergen SJA, Snijders JG, Ziegler T (2001) J Comput Chem 22:931
31. Autschbach J (2004) Calculation of heavy-nucleus chemical shifts. Relativistic all-electron methods. In: Kaupp M, Bühl M, Malkin VG (eds) Calculation of NMR and EPR parameters. Wiley-VCH, Weinheim, chap 14, p 227
32. Autschbach J, Ziegler T (2004) Relativistic calculations of spin–spin coupling constants of heavy nuclei. In: Kaupp M, Bühl M, Malkin VG (eds) Calculation of NMR and EPR parameters. Wiley-VCH, Weinheim, chap 15, p 249
33. Pregosin PS (ed) (1991) Transition metal nuclear magnetic resonance. Elsevier, Amsterdam
34. Bagno A, Bonchio M (2004) Magn Reson Chem 42:S79
35. Bagno A, Bonchio M, Sartorel A, Scorrano G (2000) Eur J Inorg Chem 17
36. Ceccon A, Santi S, Orian L, Bisello A (2004) Coord Chem Rev 248:683
37. Orian L, Bisello A, Santi S, Ceccon A, Saielli G (2004) Chem Eur J 10:4029
38. Smith PJ (ed) (1998) Chemistry of Tin. Blackie Academic & Professional, London
39. Bagno A, Casella G, Saielli G (2006) J Chem Theory Comput 2:37
40. Bagno A, Bertazzi N, Casella G, Pellerito L, Saielli G, Sciacca ID (2006) J Phys Org Chem (in press). DOI http://dx.doi.org/10.1002/poc.1041
41. Bagno A, Saielli G (2003) Chem Eur J 9:1486
42. Bagno A, Bonchio M, Sartorel A, Scorrano G (2003) ChemPhysChem 4:517
43. Bagno A, Bonchio M, Autschbach J (2006) Chem Eur J 12:8460-8471
44. Bagno A, Bonchio M (2005) Angew Chem Int Ed 44:2023
45. Autschbach JA, Igna CD, Ziegler T (2003) J Am Chem Soc 125:4937
46. Malleier R, Kopacka H, Schuh W, Wurst K, Peringer P (2001) Chem Commun 51
47. Gillespie RJ, Granger P, Morgan KR, Schrobilgen GJ (1984) Inorg Chem 23:887
48. Cutforth BD, Gillespie RJ, Ireland P, Sawyer JF, Ummat PK (1983) Inorg Chem 22:1344
49. Breuning E, Hanan GS, Romero-Salguero FJ, Garcia AM, Baxter PNW, Lehn JM, Wegelius E, Rissanen K, Nierengarten H, van Dorsselaer A (2002) Chem Eur J 8:3458
50. Grzesiek S, Cordier F, Jaravine V, Barfield M (2004) Prog NMR Spectrosc 45:275
51. Bagno A (2000) Chem Eur J 6:2925
52. Salsbury FR, Harris RA (1998) Mol Phys 94:307
53. Pecul M (2000) J Chem Phys 113:10835
54. Nishio M, Hirota M, Umezawa Y (1998) The CH/π interaction. Evidence, nature and consequences. Wiley-VCH, New York
55. Bagno A, Saielli G, Scorrano G (2001) Angew Chem Int Ed 40:2532
56. Bagno A, Saielli G, Scorrano G (2002) Chem Eur J 8:2047
57. Bagno A, Saielli G, Scorrano G (2002) ARKIVOC IV:38
58. Bagno A, Saielli G (2004) J Phys Org Chem 17:945
59. Heckman JJ, Ledbetter MP, Romalis MV (2003) Phys Rev Lett 91:067601
60. Howarth OW, Nelson J, McKee V (2000) Chem Commun 21
61. Pavone M, Brancato G, Morelli G, Barone V (2006) ChemPhysChem 7:148
62. Moon S, Patchkovskii S (2004) First-principles calculations of paramagnetic NMR shifts. In: Kaupp M, Bühl M, Malkin VG (eds) Calculation of NMR and EPR parameters. Wiley-VCH, Weinheim, chap 20, p 325
63. Luchinat C, Bertini I (2001) NMR of paramagnetic substances. Elsevier, Amsterdam
64. Frisch MJ et al. (2004) Gaussian 03. Gaussian, Inc., Wallingford
65. Becke AD (1993) J Chem Phys 98:5648
66. Lee C, Yang W, Parr RG (1988) Phys Rev B 37:785
67. Becke AD (1988) Phys Rev A 38:3098
68. Perdew JP (1986) Phys Rev B 33:8822